Heart Rate Measurement and Blur Image Quality Metric via Image Processing: An Overview

Raveendran Paramesran[1, a)] and Mohd Fikree Hassan[2, 3]

[1)]*Department of Electrical Engineering, Faculty of Engineering, University of Malaya, 50603 Kuala Lumpur, Malaysia.*
[2)]*Institute of Computer Science and Digital Innovation, UCSI University, 56000 Cheras, Kuala Lumpur, Malaysia.*
[3)]*Faculty of Arts and Sciences, International University of Malaya-Wales, 50480 Kuala Lumpur, Malaysia.*

[a)]*Corresponding author: ravee58@gmail.com*

Abstract. The research area of image processing and its applications has significantly increased in the last decades. They can be found in medical imaging, military, surveillance, astronomy, sports, and many more. In this paper, we show two applications of image processing; heart rate measurement and a no-reference blur image quality metric. The heart rate measurement is obtained from video sequences. However, the heart rate measurement consists of artifacts and noises. Therefore, a novel method using the Canonical Component Analysis (CCA) is introduced to eliminate the artifacts and noises using two five-second video frames where one video is delayed by one second. In a no-reference blur image quality metric, we show that some exact Zernike moments (EZMs) closely exhibit the human visual system in assessing the quality of images distorted by various degrees of Gaussian blur. These EZMs are then combined through a formulation and trained using a support vector machine to give the quality scores for images from the widely used public databases.

INTRODUCTION

During the early days of computing, data was numerical and textual. Currently, data comes in many forms, such as voice, speech, music, image, and many more. Each of these forms is considered a signal that carries information. Due to the pandemic, the usage of communication devices has increases, and images play an important function in our daily activities. Images carry information and are used in communication among people. Hence, the usage of images in distributing information via websites and smartphone applications has increased in the 21st century as millions of images are shared on the Internet every day.

An image is an object that portrays visual perception and can be represented as a two-dimensional function as below.

$$I = f(x,y), \tag{1}$$

where I is the image, x and y are spatial coordinates, and the amplitude of f represent the intensity or gray-level of the image which typically range from 0 to 255. All these numbers are considered data that we can process and transform to achieve certain objectives and solutions to certain problems.

This transformation process is also known as image processing, a research field that provides enhanced image information that can be used for human understanding and machine perception. It implements techniques to process the raw or corrupted images and obtains meaningful information. Its applications can be found in various areas such as human color vision [1], surveillance [2], image restoration [3], and many more.

In this paper, we will review and summarize two applications of image processing; heart rate measurement [4] and blur image quality metric [6]. These two applications were chosen because we want to show that image processing is a diverse research area covering a variety of applications. Besides image-based applications, it is also used in video-based applications and quality assessment processes.

Human heart rate is one of the parameters in sports and healthcare [4]. Conventionally, heart rate is measured using an Electrocardiography (ECG) machine, a contact-based method. It uses the electrodes that are attached around the wrist and chest area. Although this is the most common method to measure heart rate, patients with sensitive skins might not be suitable to this method [5]. Therefore, non-contact-based methods are proposed as an alternative to the ECG machine.

One of the non-contact-based methods for heart rate measurement is via facial images obtained from video sequences. However, the heart rate measured has random artifacts and noises. Ling et al. [4] proposed a novel method using the Canonical Component Analysis (CCA) to minimize the artifacts and noises. They considered that two video durations contain the heart rate signals that are strongly correlated between them, while the random artifacts and noises are not correlated to each other.

First International Conference on Computational Science & Data Analytics
AIP Conf. Proc. 2756, 020002-1–020002-9; https://doi.org/10.1063/5.0140251
Published by AIP Publishing. 978-0-7354-4566-6/$30.00

In this method, they identify the heart rate by maximizing the correlation of the two five-second video frames. The obtained heart rate is then passed to a bandpass filter followed by the Fast Fourier Transform (FFT). Then, the heart rate signal is chosen from the highest peak between the RGB sources.

In image processing research field, one of the challenges is the relevance of feature extraction for image analysis [6]. Since the introduction of geometric moments [7], orthogonal moments such as Legendre moments [8], Zernike moments [8], Tchebichef moments [9], and Krawtchouk moments [10], have been used in feature extraction. Orthogonal moments are good signal descriptors and have been widely use in various applications such as object classification [15], biometric [16], biomedical imaging [17], and image quality assessment [18].

Lim et al. [6] proposed a no-reference blur metric based on the identified exact Zernike moments (EZMs) together with the gradient magnitude (GM). They utilized EZMs to eliminate the numerical errors from the computations of Zernike moments. In their method, they derived a set of EZMs that closely exhibit human quality scores for images with different levels of blurriness. Due to the similarity, they formulated a no-reference blur metric using the EZMs and GM, which acts as a weight to encode the contrast information.

The rest of this paper is organized as follows. Section 2 summarizes the two applications, while section 3 provides the experimental results. Section 4 concludes the paper.

APPLICATIONS OF IMAGE PROCESSING

In this section, we summarize the two applications of image processing; the CCA based heart rate measurement [4], and the EZM based blur image quality metric [6].

CCA Based Heart Rate Measurement

Heart rate obtained from contact-based methods has random artifacts and noises. Ling et al. [4] proposed a novel method utilizing the Canonical Component Analysis (CCA) to overcome this issue. They started by determining the Region of Interest (ROI) as defined in [11] and computed the mean values of the red (R), green (G), and blue (B) components. Using the algorithm proposed by Tarvainen et al. [12], the mean values were detrended. Then, they applied the Canonical Component Analysis Blind Source Separation (CCABSS) [13] to find the original source for all three R, G, and B components.

Next, they applied CCA to the two detrended five-second video frames. One of the video frames is delayed by a second. Then, they rescaled the singular output of the CCA block in order to maximize the amplitude of the signals. It is achieved by minimizing the effect of different amplitudes. After the rescaling, the signals are passed through a bandpass filter. The output signals are then transformed into the frequency domain using FFT, and the highest peak is determined as the heart rate value. The overall process flow is illustrated in Fig. 1.

CCA is utilized to determine the relationship between two sets of variables. It aims to maximize the correlations between objects represented with the two data. In the CCA based heart rate measurement, A and B denote the data obtained from the two five-second video frames where A is the first and B is the second. The camera records 50 frames per second, thus, there are 250 frames for each data. Hence, A and B are expressed as below.

$$A = [\mu(t_1), ..., \mu(t_{250})], \tag{2}$$

$$B = [\mu(t_{51}), ..., \mu(t_{300})], \tag{3}$$

where $\mu(t_n)$ is the video frame sequences and t_n is the frame sequence number.

CCA will determine the relationship between A and B by computing their correlation values, ρ. Since the different between B and A is one second, the heart rate is considered to vary insignificantly. It is also assumed that these two five-second video frames contain the heart rate signals that are strongly correlated. Moreover, the random artifacts and noises appearing in both video frames are not correlated to each other. Thus, the desired heart rate will remain unchanged, which gives maximum correlation values. To determine the desired original sources, the eigenvalues and eigenvectors obtained with the maximum correlation values are multiplied with the source A.

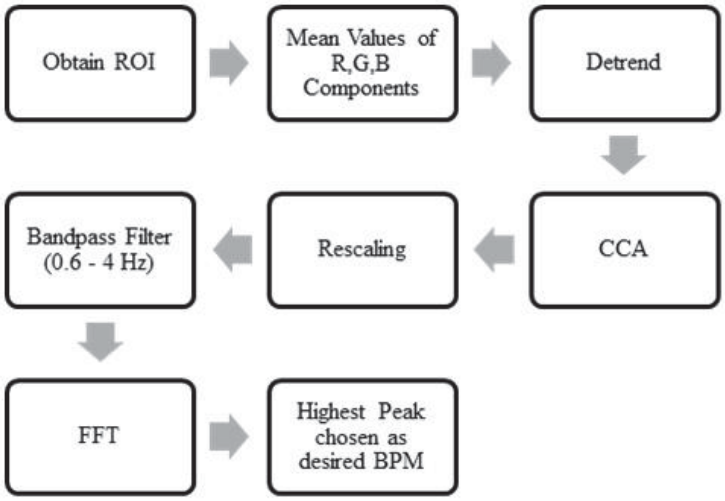

FIGURE 1: Process flow of CCA heart rate measurement.

EZM Based Blur Image Quality Metric

An important characteristic in constructing a blur image quality metric is the features that closely model the human perception for images with varying degrees of blurriness. Lim et al. [6] successfully showed that some of the EZMs can do this and can be considered as edge descriptors. Moreover, they chose EZMs because they solve the existence of the numerical errors arising from the computation of ZMs [14].

The EZMs of order p and repetition q can be computed using the equation below.

$$EZM_{p,q} = \frac{p+1}{\pi} \sum_{\substack{k=q,\\ p-k=even}}^{p} \sum_{m=0}^{s} \sum_{n=0}^{q} (-\hat{j})^n \times \binom{s}{m} \binom{q}{n} B_{p,q,k} EGM_{k-2m-n,2m+n}, \tag{4}$$

where $B_{p,q,k}$ is calculated using Coefficient Method in [19], $\hat{j} = \sqrt{-1}$, $EGM_{k-2m-n,2m+n}$ is the exact geometric moment.

The relationship between EZMs for the original image $EZM^{(f)}_{p,q}$, the blur image $EZM^{(g)}_{p,q}$, and the point spread function, PSF $EZM^{(h)}_{p,q}$ is given as below.

$$EZM^{(g)}_{p,q} = \sum_{i=0}^{l} EZM^{(f)}_{q+2i,q} \sum_{j=0}^{l-i} EZM^{(h)}_{2j,0} \sum_{k=i+j}^{l} \sum_{n=i}^{k-j} \binom{q+k}{q+n} \binom{k}{n} c^q_{l,k} d^q_{n,i} d^0_{k-n,j}, \tag{5}$$

where c and d are given by

$$c^q_{l,k} = (-1)^{l-k} \frac{q+2l+1}{\pi} \frac{(q+l+k)!}{k!(l-k)!(q+k)!}, \tag{6}$$

$$d^q_{i,j} = \frac{i!(q+i)!\pi}{(i-j)!(q+i+j+1)!}, \tag{7}$$

Then, they measure the contrast information by computing the GM. The GM was used as a weight in their blur image quality metric. The development of the blur image quality metric consists of two stages. In the first stage, the EZM differences and the GM dissimilarities between the edge points of the test image and the same re-blurred image were extracted. In the second stage, the mean of the weighted EZM features is then pooled into a single blur index to quantify the image quality via a support vector machine regressor (SVR). The overall process flow is illustrated in Fig. 2.

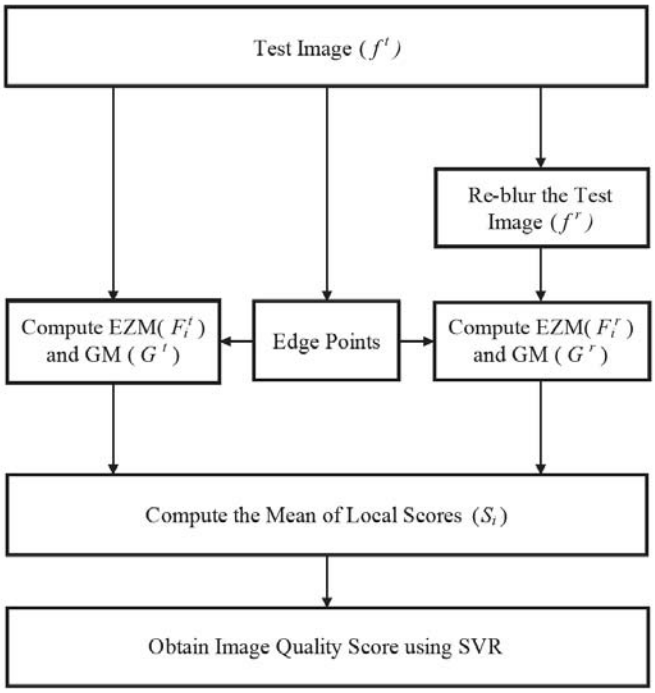

FIGURE 2: Process flow of EZM based blur image quality metric.

From Figure 2, the EZMs of the test and blurred images are represented by F^t and F^r, respectively. Meanwhile, the GMs are denoted by G^t and G^r for the two images. The test image is convolved with the edge operator kernel. Using the adaptive thresholding and based on the edge strengths, the actual edge points are obtained. Then, the edge map of the test image is constructed. Based on the edge map, each edge point is used as the center of a 3×3 block. Next, F^t and G^t are computed for every block centered at the edge point.

At the same time, the test image is reblurred using a Gaussian blur kernel. Because the differences are measured at the same location between the test and reblurred image, F^r and G^r are computed based on the edge points extracted from the test image.

For every edge point, the absolute difference of the EZMs, S_{F_i} for $1 = 1,2,...,6$, and the dissimilarity of the GM, S_G are computed as follow:

$$S_{F_i}(k) = \left|F_i^t(k) - F_i^r(k)\right|, \tag{8}$$

$$S_G(k) = 1 - \frac{2G^t(k) \cdot G^r(k)}{(G^t(k))^2 + (G^r(k))^2}, \tag{9}$$

where $k = 1,2,...,K, K$ is the number of edge point of the test image.

The local scores, S_{L_i}, for $1 = 1,2,...,6$, are computed using

$$S_{L_i}(k) = [S_G(k)]^{\alpha} \cdot [S_{F_i}(k)]^{\beta}, \tag{10}$$

where α and β are the parameters to adjust the relative importance of EZM and GM features. Then, the overall score of the test images is computed by taking the mean values of the local scores.

$$S_i = \frac{\sum_{k=1}^{K} S_{L_i}(k)}{K}, \tag{11}$$

Lastly, the mean values are fed to a trained support vector machine regressor to assign the quality scores.

EXPERIMENTAL RESULTS

In this section, we present the experimental results of the two applications. There are two experiments conducted for each application.

CCA Based Heart Rate Measurement

For the CCA based Heart Rate Measurement, two experiments were conducted; increasing and decreasing heart rate variation with video duration varied between 5 and 7 seconds. It is assumed that during this duration, the video frames contain the heart rate signals that are strongly correlated to each other. Moreover, the random artifacts and noises appearing in the video frames during this duration are not correlated to each other. Therefore, the experiment utilized 5 seconds and 7 seconds durations. The results were compared with the independent component analysis (ICA) based method.

Eight volunteers were involved in these experiments, and they wore the Polar Heart Rate Monitor - Polar Team^2 Pro to measure their instantaneous heart rates as a reference during both experiments. A Sony camcorder (HDR-PJ260VE) with 50 frames per second and 24-bit RGB (with 8 bits per channel) was used for video recording. The camcorder was placed and fixed at 0.60m from the volunteer's face. The experiment used the Viola and Jones model to detect the face region. Moreover, the ROI is determined to be the area below the eyes and above the upper lips of the mouth in a video frame.

Increasing Heart Rate

During this experiment, the volunteers were asked to cycle at different speeds for about two minutes to get their heart rate to increase. Then, their facial were recorded for one minute and during this period, they must continue to cycle with minimum movement. For each volunteer, a total of 60 readings were obtained, and a comparison was made to the actual heart rate reading.

Results of the Root Mean Square Error (RMSE) and Pearson coefficients for each subject for both the CCA and ICA based methods for 5 and 7 seconds video duration are shown in Tables I and II. Lower RMSE values indicate lower error in the video sequence, while higher Pearson coefficients indicate a high correlation between the video frames. It can be observed that CCA based method gives better results when compared to ICA based methods for both 5 and 7 seconds video duration.

TABLE I: Results for 5 seconds video duration

Subject	Heart Rate Value (BPM)		RMSE		Pearson coefficient	
	Starting	Ending	CCA	ICA	CCA	ICA
1	98	111	3.16	3.74	0.67	0.72
2	83	96	4.29	4.05	0.59	0.64
3	84	122	3.19	11.25	0.98	0.73
4	95	130	2.11	18.83	0.99	0.34
5	101	124	5.87	19.35	0.83	0.11
6	93	144	1.78	8.98	0.99	0.88
7	112	139	1.20	13.69	0.99	0.37
8	111	132	5.26	22.27	0.95	0.12

Decreasing Heart Rate

In this experiment, the volunteers were asked to cycle at high speed to raise their heart rates to a high level. When a significant heart rate is achieved, the volunteers were asked to stop cycling and they must stay still with no motion for one minute. During this period, the camcorder captured their facial images.

TABLE II: Results for 7 seconds video duration

Subject	Heart Rate Value (BPM)		RMSE		Pearson coefficient	
	Starting	Ending	CCA	ICA	CCA	ICA
1	103	112	1.59	1.68	0.74	0.69
2	83	96	3.04	3.27	0.72	0.68
3	84	125	1.70	2.01	0.99	0.99
4	96	130	1.24	3.22	0.99	0.96
5	101	136	5.14	13.09	0.93	0.34
6	95	130	1.25	1.98	0.99	0.98
7	101	138	4.94	9.20	0.93	0.61
8	86	128	1.50	2.47	0.99	0.98

Results of the Root Mean Square Error (RMSE) and Pearson coefficients for each subject for both the CCA and ICA based methods for 5 and 7 seconds video duration are shown in Tables III and IV. It can be observed that CCA based method gives better results when compared to ICA based methods for both 5 and 7 seconds video duration.

TABLE III: Results for 5 seconds video duration

Subject	Heart Rate Value (BPM)		RMSE		Pearson coefficient	
	Starting	Ending	CCA	ICA	CCA	ICA
1	115	97	1.40	2.78	0.98	0.90
2	94	71	2.02	2.03	0.96	0.97
3	153	121	1.39	1.64	0.99	0.98
4	145	128	3.75	10.67	0.75	0.29
5	151	116	2.58	13.64	0.96	0.67
6	153	121	1.64	1.88	0.99	0.99
7	151	115	1.87	13.21	0.98	0.51
8	145	126	2.92	16.22	0.86	0.31

TABLE IV: Results for 7 seconds video duration

Subject	Heart Rate Value (BPM)		RMSE		Pearson coefficient	
	Starting	Ending	CCA	ICA	CCA	ICA
1	115	97	1.62	1.93	0.97	0.96
2	94	71	1.50	1.88	0.98	0.97
3	153	121	2.28	2.41	0.99	0.99
4	145	126	3.21	5.32	0.84	0.70
5	153	121	1.89	2.09	0.99	0.99
6	151	114	1.43	1.90	0.99	0.98
7	144	126	2.18	2.23	0.90	0.90
8	151	114	1.88	2.31	0.99	0.99

In both experiments, the results implies that the video duration needs to be increased for the ICA based-method for it to have a lower error which is not the case for the CCA based-method [4]. Also, it is observed that the video frames for CCA based-method have higher correlation compared to the ICA based-method.

EZM Based Blur Image Quality Metric

For the EZM based blur image quality metric, two experiments were conducted. The first experiment was a comparative analysis with existing blur metrics using the LIVE [20], TID2008 [21] and CSIQ [22] image databases. A dependency test was performed in the second experiment to check the robustness of the metric.

The LIVE database consists of 145 Gaussian blur distorted images generated from 29 different color images applying five different levels of distortion. Meanwhile, the CSIQ and TID2008 databases have 30 and 25 color reference images, respectively. There are five levels of Gaussian blur distortion applied to the CSIQ reference image and there are four levels of Gaussian blur distortion applied to the TID2008 reference images.

The Difference Mean Opinion Scores (DMOS) were provided by LIVE and CSIQ databases. Meanwhile, the Mean Opinion Scores (MOS) were provided by the TID2008 database. Since all three databases have different DMOS and MOS values, the DMOS of CSIQ and the MOS of TID2008 databases were rescaled to the range of DMOS for the LIVE database.

Comparative Analysis with Existing Blur Metrics

In this experiment, EZM based blur image quality metric (EZMBM) was compared with existing no-reference (NR) algorithms. In addition, it was also compared to five full-reference (FR) algorithms.

The Pearson's correlation coefficient (CC) and Spearman's rank-ordered correlation coefficient (SROCC) between the predicted score are employed to evaluate the performance. CC indicates the prediction accuracy after the linear/non-linear regression, whereas SROCC predicts monotonicity. A value close to 1 for CC and SROCC indicates good performance for the blur metric.

Table V shows the results between the EZMBM and the FR and NR blur metrics for Gaussian blur images from the LIVE database. For the FR blur metric, the EZMBM performs better than others except for FSIM and FSIMc. Meanwhile, a comparison between the NR blur metrics shows that the EZMBM outperforms them for both scores. The rotation invariance property of the EZM caused the features to not be affected by the direction of the edges. Hence, it gave the EZMBM an advantage over others. Moreover, the EZMBM correlates much more consistently with the subjective evaluation than others.

TABLE V: Performance Comparison with FR and NR Blur Metrics for LIVE Database

Blur Metrics	Type	CC	SROCC
PSNR	FR	0.7993	0.7734
SSIM [23]	FR	0.8740	0.8942
MS-SSIM [24]	FR	0.9485	0.9516
FSIM [25]	FR	0.9722	0.9710
FSIMc [25]	FR	0.9723	0.9711
Li et al. [26]	NR	0.9329	0.9252
JNBM [27]	NR	0.7431	0.7521
CPBD [28]	NR	0.9033	0.9053
GPVM [29]	NR	0.8800	0.8750
BLIIND-II [30]	NR	0.8994	0.8912
DIIVINE [31]	NR	0.9370	0.9373
BRISQUE [32]	NR	0.9506	0.9511
M_3 [33]	NR	0.9221	0.8759
ZMBM	NR	0.9635	0.9588
EZMBM	NR	0.9659	0.9625

Table VI show the results between the EZMBM and the NR blur metrics for Gaussian blur images from the CSIQ and TID2008 databases. It can be observed that the performance of the EZMBM is competitive as compared to the other NR blur metrics for the both databases.

Dependency Test

In this experiment, the robustness of the EZMBM is evaluated via a dependency test. The dependency test is conducted by testing the performance of the EZMBM learned from one database and tested on another database. First, the EZMBM was trained on the LIVE database and tested on the TID2008 and CSIQ databases.

TABLE VI: Performance Comparison with FR and NR Blur Metrics for CSIQ and TID2008 Databases

Blur Metrics	CSIQ		TID2008	
	CC	SROCC	CC	SROCC
BLIIND-II	0.9003	0.9082	0.8982	0.9219
DIIVINE	0.8697	0.9010	0.8930	0.9038
BRISQUE	0.9085	0.9356	0.9357	0.9391
M_3	0.9243	0.9457	0.9369	0.9406
EZMBM	0.9285	0.9333	0.9323	0.0409

Then, it was trained on the TID2008 database and tested on LIVE and CSIQ databases. Lastly, it was trained on the CSIQ database and tested on LIVE and TID2008 databases. The training-testing procedures are applied to the other three existing NR blur metrics for comparison, and the results are illustrated in Table VII. The results show that the EZMBM performance is comparable to the three NR blur metrics.

TABLE VII: Performance Comparison with FR and NR Blur Metrics for CSIQ and TID2008 Databases

Training Database	Testing Database	DIVINE	BLIIND-II	BRISQUE	M_3	EZMBM
LIVE	CSIQ	0.8571	0.8878	0.8993	0.9108	0.8986
LIVE	TID2008	0.8599	0.9056	0.9050	0.9204	0.8393
TID2008	LIVE	0.8658	0.9389	0.9228	0.9336	0.9200
TID2008	CSIQ	0.8481	0.8747	0.8665	0.8393	0.8672
CSIQ	LIVE	0.8475	0.9365	09311	0.9459	0.9367
CSIQ	TID2008	0.8223	0.8005	0.8986	0.9051	0.8409

CONCLUSION

This paper presented two applications of image processing: CCA based heart rate measurement and EZM based blur image quality metric. The CCA based heart rate measurement is a non-contact-based method that minimizes the artifacts and noises. The heart rate was obtained from video sequences, and it is assumed that a small delayed of one-second video duration from the first video duration will contain the heart rate signals that are strongly correlated. Meanwhile, the artifacts and noises appearing in both video frames are not correlated to each other. Comparison between CCA and ICA based heart rate measurement shows that the CCA based method produces better heart rate measurement.

On the other hand, the EZM based blur image quality metric provides an advantage that the features will not be affected by the direction of the edges due to the rotation invariance property of EZM. Experimental results show that the EZM based blur image quality metrics perform better than other NR blur metrics. Therefore, the EZM based method correlates well with human evaluation on digital images with various blur degrees.

REFERENCES

1. M. F. Hassan, Int. J. Image Graph. **21**, 2150004 (2021).
2. M. Patel, A. Yadav, C. Valderrama, Soft Computing for Security Applications, Springer Singapore, 733 (2022).
3. M Yin, T. Adam, R. Paramesran, M. F. Hassan, Signal Process. Image Commun. **102**, 116620 (2022).
4. S. S. Ling, R. Paramesran, Y. P. Yu, Adv. in Electrical and Computer Engineering, **19**, 41 (2019).
5. D. Teichmann, C. Brüser, B. Eilebrecht, A. Abbas, N. Blanik, S. Leonhardt, In Annu. Int. Conf. IEEE Eng. Med. Biol. Soc., IEEE, 1302 (2012).
6. C. L. Lim, R. Paramesran, W. A.Jassim, Y. P. Yu and K. N. Ngan, J. of the Franklin Institute, **353**, 4715 (2016).
7. M. K. Hu, IRE Trans. Inf. Theory **8**, 179 (1962).
8. M. R. Teague, J. Opt. Soc. Am. **70**, 920 (1980).
9. R. Mukundan, S. Ong, P. A. Lee, IEEE Trans. Image Process. **10**, 1357 (2001).
10. P. T. Yap, R. Paramesran, S. H. Ong, IEEE Trans. Image Process. **12**, 1367 (2003).

11. T. Pursche, J. Krajewski, R. Moeller, In Proceedings of IEEE International Conference on Consumer Electronics, IEEE, 544 (2012).
12. M. P. Tarvainen, P. O. Ranta-aho, P. A. Karjalainen, IEEE Transactions on Biomedical Engineering **49**, 172 (2002).
13. M. Borga, H. Knutsson, Linköping University, Linköping, Sweden, Technical Report LiU-IMT-EX-0062 (2001).
14. C. Y. Wee, R. Paramesran, R. Mukundan, X. Jiang, Pattern Recognition **43**, 4055 (2010).
15. S. Erasmus, K. Smith, J. of Microscopy **127**, 185 (1982).
16. G. Amayeh, G. Bebis, A. Erol, M. Nicolescu, In: 2006 Conference on Computer Vision and Pattern Recognition Workshop, CVPRW'06, 40 (2006).
17. L. Wang, H. Ling, F. Zou, Z. Lu, Z. Wang, Comput. Methods Programs. Biomed. **95**, 10 (2009).
18. K. H. Thung, R. Paramesran, C. L. Lim, Pattern Recognition **45**, 2193 (2012).
19. C. W. Chong, R. Mukundan, R. Paramesran, In: Proceedings of the 6th Joint Conference on Information Science, JCIS'02, Research Triangle Park, NC, 785 (2002).
20. H. Sheikh, Z. Wang, L. Cormack, A. Bovik, Live Image Quality Assessment Database Release 2 [online], http://live.ece.utexas.edu/research/quality/subjective.htm, (2005).
21. N. Ponomarenko, K. Egiazarian, Tampere Image Database 2008 (TID2008) [online], http://www.ponomarenko.info/tid2008.htm, (2008).
22. E. Larson, D. M. Chandler, Categorical Image Quality (CSIQ) Database 2009 [on-line], http://vision.okstate.edu/csiq, (2009).
23. Z. Wang, A. Bovik, H. Sheikh, E. Simoncelli, IEEE Trans. Image Process. **13**, 600 (2004).
24. Z. Wang, E. P. Simoncelli, A. C. Bovik, In: Conference Record of the Thirty-Seventh Asilomar Conference on Signals, Systems and Computers **2**, IEEE, 1398 (2004).
25. L. Zhang, D. Zhang, X. Mou, IEEE Trans. Image Process. **20**, 2378 (2011).
26. C. Li, W. Yuan, A. Bovik, X. Wu, Electronics Letters **47**, 962 (2011).
27. R. Ferzli, L. Karam, IEEE Trans. Image Process. **18**, 717 (2009).
28. N. Narvekar, L. Karam, IEEE Trans. Image Process. **20**, 2678 (2011).
29. F. Crete, T. Dolmiere, P. Ladret, M. Nicolas, Human Vision and Electronic Imaging XII **6492**, (2007).
30. M. A. Saad, A. C. Bovik, C. Charrier, IEEE Trans. Image Process. **21**, 3339 (2012).
31. A. K. Moorthy, A. C. Bovik, IEEE Trans. Image Process. **20**, 3350 (2011).
32. A. Mittal, A. K. Moorthy, A. C. Bovik, IEEE Trans. Image Process. **21**, 4695 (2012).
33. W. Xue, X. Mou, L. Zhang, A. C. Bovik, X. Feng, IEEE Trans. Image Process. **23**, 4850 (2014).